

DOI: 10.1177/0003702819892646

# External Cavity Quantum Cascade Laser-Based Mid-Infrared Dispersion Spectroscopy for Qualitative and Quantitative Analysis of Liquid-Phase Samples

Stefan Lindner<sup>1</sup>, Jakob Hayden<sup>1</sup>, Andreas Schwaighofer<sup>1</sup>, Tobias Wolflehner<sup>1</sup>,  
Christian Kristament<sup>1</sup>, María González-Cabrera<sup>2</sup>, Stefan Zlabinger<sup>1</sup>, and Bernhard Lendl<sup>1\*</sup>

<sup>1</sup> Institute of Chemical Technologies and Analytics, Vienna University of Technology, Getreide-  
markt 9/164-UPA, 1060 Vienna, Austria

<sup>2</sup> Department of Physical and Analytical Chemistry, Universidad de Jaén, Campus Las  
Lagunillas, s/n, 23071, Jaén, Spain

**Corresponding author email:** [Bernhard.lendl@tuwien.ac.at](mailto:Bernhard.lendl@tuwien.ac.at)

## ABSTRACT

Acquisition of classical absorption spectra of liquids in the mid-IR range with quantum cascade lasers (QCLs) is often limited in sensitivity by noise from the laser source. Alternatively, measurement of molecular dispersion (i.e., refractive index) spectra poses an experimental approach that is immune to intensity fluctuations and further offers a direct relationship between the recorded signal and the sample concentration. In this work, we present an external cavity quantum cascade laser (EC-QCL) based Mach–Zehnder interferometer setup to determine dispersion spectra of liquid samples. We present two approaches for acquisition of refractive index spectra and compare the qualitative experimental results. Furthermore, the performance for quantitative analysis is evaluated. Finally, multivariate analysis of a spectrally complex mixture comprising three different sugars is performed. The obtained figures of merit by partial least squares (PLS) regression modelling compare well with standard absorption spectroscopy, demonstrating the potential of the introduced dispersion spectroscopic method for quantitative chemical analysis.

**Keywords:** Mid-infrared spectroscopy, mid-IR spectroscopy, dispersion spectroscopy, quantum cascade laser, QCL, liquid phase

## INTRODUCTION

In the mid-infrared (mid-IR) region ( $400\text{--}4000\text{ cm}^{-1}$ ) organic molecules possess their strongest rotational–vibrational transitions, thus offering highly discriminatory information inherently allowing molecule specific detection. Currently, the most widespread type of mid-IR spectroscopy for routine quantitative and qualitative analysis is absorption spectroscopy in the form of Fourier transform IR (FT-IR) spectroscopy because of its versatility and simplicity. In absorption spectroscopy, attenuation of the radiation intensity caused by an absorption process is measured. This relies on detecting small signal changes due to absorption of the analyte on top of a large background, i.e., the total light intensity arriving at the detector. General drawbacks of absorption spectroscopy arise from a direct impact of the intensity noise on the measured absorption signal and possible dynamic range limitations due to eventual nonlinearities of the detectors used.<sup>1–3</sup> For thermal light sources employed in FT-IR spectroscopy, these intensity fluctuations can usually be neglected, however, their low emission power constitutes a disadvantage for many applications.

More than two decades ago, the first quantum cascade lasers (QCLs) were introduced as a high-intensity light source for the mid-IR region. QCLs provide polarized and coherent light with spectral power densities several orders of magnitude higher than thermal light sources.<sup>4,5</sup> For liquid phase applications, the highly available emission power was the first of these unique characteristics that was exploited to implement direct absorption setups. The high laser intensities allowed to increase optical paths of transmission measurements compared to FT-IR spectroscopy,<sup>6</sup> particularly after emergence of external cavity (EC)-QCLs that provide spectral tuning ranges of several hundred wavenumbers.<sup>7–9</sup> However, recently reported EC-QCL based systems offer increased ruggedness compared to FT-IR spectroscopy at only slightly better signal-to-noise ratios (SNR)<sup>10</sup> owing to the high noise levels introduced by the laser light sources.

Very recently, an EC-QCL was combined with a Mach–Zehnder interferometer (MZI) for proof-of-principle measurements of broadband dispersion (refractive index) spectra in the mid-IR spectral region.<sup>11</sup> In dispersion spectroscopy, the phase shift of the radiation due to passing through a sample is measured. Dispersion and absorption are caused by the same process, thus the same spectral information about the sample can be retrieved by determining either of the two

properties. Approaches to measuring molecular dispersion using QCLs were reported for applications in the gas phase using chirped laser dispersion spectroscopy (CLaDS),<sup>12</sup> and recently also using a new variant entitled heterodyne phase sensitive dispersion spectroscopy (HPSDS). Measuring anomalous dispersion at a molecular resonance rather than its absorption yields the advantage of independence of signals from laser power and a linear relationship between dispersion signals and sample concentration, even for optically thick samples.<sup>13</sup> Particularly the former aspect holds promise for applications of QCLs that emit with comparably high intensity noise.

In this work, we present an EC-QCL based MZI setup for acquisition of broadband refractive index spectra. MZIs are well known for refractive index sensing at single wavelengths from biosensing applications in wavelength regions from the visible to the mid-IR,<sup>14-16</sup> but their application to broad band mid-IR dispersion spectroscopy is yet pending. In the presented approach, the MZI is operated at an optical phase difference of  $\frac{\pi}{2}$  to record phase shifts at highest sensitivity induced by the sample and reference placed inside the interferometer arms. We present two approaches for acquisition of refractive index spectra. One method employs active compensation of the sample induced phase shift using a mirror mounted on a piezo actuator, whereas the second method requires no moving parts. Whereas the first method (moving piezo method) appears to be more accurate from a metrological point of view the second method (fixed piezo method) entails the advantage of being more rugged as no moving parts are involved. After comparison and discussion of the qualitative experimental results, the performance of the latter approach for quantitative analysis is evaluated. Finally, multivariate analysis of a mixture of three different sugars is performed to demonstrate the capability of dispersion spectroscopy to tackle challenging analytical problems.

## EXPERIMENTAL

### Basic Principles of Mach–Zehnder Interferometer-Based Dispersion Spectroscopy.

Generally, the intensity output  $I_{out}$  of a two-beam interferometer such as the MZI discussed herein can be expressed as

$$I_{\text{out}} = I_a + I_b + 2\sqrt{I_a I_b} \cos(\Delta\varphi) \quad (1)$$

where  $I_a$  and  $I_b$  are the intensities of the two interfering waves (measured at the detectors D1 and D2) and  $\Delta\varphi$  is the phase shift between them. For the interferometric setup shown in Figure 1, the interfering waves yielding the signal at Detector 1 are characterized by the intensities and relative phase

$$I_{a,1} = I_0 T^2 10^{-A_0} \quad (2)$$

$$I_{b,1} = I_0 R^2 10^{-(A_0+A)} \quad (3)$$

$$\Delta\varphi_1 = \frac{2\pi}{\lambda} [\Delta l + (n - n_0)d] \quad (4)$$

Herein,  $I_0$  is the laser intensity,  $T$  and  $R$  are the transmittance and reflectivity of the beam splitters (assumed equal),  $10^{-A_0}$  denotes the attenuation of the reference liquid in flow cell FC1, and  $A$  is the absorption of the sample in flow cell FC2 with respect to the reference. Furthermore,  $\lambda$  indicates the wavelength,  $\Delta l$  is the geometric path length difference between the two interferometer arms,  $n$  and  $n_0$  are the refractive indices of the sample (FC2) and reference (FC1) cell and  $d$  is the equal film thickness of the two flow cells.

For Detector D2, the interfering waves are described by

$$I_{a,2} = I_0 R T 10^{-A_0} \quad (5)$$

$$I_{b,2} = I_0 R T 10^{-(A_0+A)} \quad (6)$$

$$\Delta\varphi_2 = \Delta\varphi_1 - \pi \quad (7)$$

The difference of  $\pi$  between  $\Delta\varphi_1$  and  $\Delta\varphi_2$  originates from the different numbers of reflections (see Figure 1: D1 receives beams with even numbers of reflections, D2 with odd numbers of reflections, yielding a phase difference of  $\pi$  due to the fact that every reflection causes a phase shift of  $\pi$ ) and yields the antisymmetric behavior of the two interferometer outputs with respect to phase. Inserting Eq. 2 to Eq. 7 in Eq.1 yields

$$I_{\text{out},1} = I_0 10^{-A_0} \left[ T^2 + R^2 10^{-A} + 2RT 10^{-\frac{A}{2}} \cos\left(\frac{2\pi}{\lambda} [\Delta l + (n - n_0)d]\right) \right] \quad (8)$$

$$I_{\text{out},2} = I_0 10^{-A_0} \left[ RT(1 + 10^{-A}) - 2RT 10^{-\frac{A}{2}} \cos\left(\frac{2\pi}{\lambda} [\Delta l + (n - n_0)d]\right) \right] \quad (9)$$

Assuming  $R=T=0.5$ , which is valid for beam splitters with sufficiently good performance of a 50:50 splitting ratio, delivers for the normalized differential detector signal

$$\Delta I_{\text{rel}} := \frac{I_{\text{out},1} - I_{\text{out},2}}{I_{\text{out},1} + I_{\text{out},2}} = \frac{\cos\left(\frac{2\pi}{\lambda} [\Delta l + (n - n_0)d]\right)}{\frac{1}{2} \left( 10^{\frac{A}{2}} + 10^{-\frac{A}{2}} \right)} \quad (10)$$

With  $\Delta l = \frac{\lambda}{4}$ , which is fulfilled experimentally by holding mirror M1 in this position with a piezo drive, the expression for  $\Delta I_{\text{rel}}$  can be further simplified to receive

$$\Delta I_{\text{rel}} \approx \frac{2}{10^{\frac{A}{2}} + 10^{-\frac{A}{2}}} \sin\left(\frac{2\pi d}{\lambda} (n - n_0)\right) \quad (11)$$

Furthermore, this expression can be approximated by

$$\Delta I_{\text{rel}} \approx \frac{2\pi d}{\lambda} (n - n_0) \quad (12)$$

when assuming small values for the absorption  $A \approx 0$  and small differences in refractive index  $n$ -

$n_0$ , since  $\sin x \approx x$  for small values of  $x$ . Both approximations are valid for low analyte concentrations. This delivers a linear dependence of the measured signal from the refractive index, which is the basis for one of the two methods we developed (see Figure 2). In order to obtain signals that scale linearly with phase shift and hence concentration, the interferometer was operated at or around the indicated working point in Figure 2, corresponding to a phase of  $\frac{\pi}{2}$ .

### *Experimental Setup*

The experimental setup is depicted schematically in Figure 1. It consists of a Mach–Zehnder type interferometer with a flow cell integrated in each of the beam paths. The laser beam emitted by a thermoelectrically cooled external cavity quantum cascade laser (Daylight Solutions Inc., San Diego, USA; Model No. 11088, laser head: 1240–890  $\text{cm}^{-1}$ , laser Driver 1001-TLC) was split at a ratio of R:T = 48:52 by a ZnSe beam splitter (Thorlabs BSW710). Both, the reflected and transmitted beam, pass 50  $\mu\text{m}$  liquid flow cells (1" BaF<sub>2</sub> windows with PTFE spacer, Korth Kristalle GmbH), and are recombined with another beam splitter (identical to first beam splitter) and mirror before getting focused on two pyroelectric detectors (Infratec LME-336, detectivity  $4.0 \cdot 10^8 \text{cm}\sqrt{\text{Hz}}/W$  at 500 K, aperture size 5 mm diameter) by two parabolic gold mirrors (Thorlabs MPD229M01). To minimize fringing, the detectors were mounted in an angle of approximately 30 degrees to the beam. One of the mirrors in the interferometer is glued to a piezo actuator (3.6  $\mu\text{m}$  maximum displacement) connected to a commercial piezo controller (Thorlabs MDT644A) The laser was operated at a repetition rate of 100 kHz with a duty cycle of 5% and an over modulated square wave with a frequency of 100 Hz (train of pulses). The recorded detector signals were amplified and filtered with a custom-built lock-in amplifier synchronized to the 100 Hz modulation of the laser before being digitized by a NI DAQ-ADC (Model 9205, National Instruments Corp.).

### *Recording of Dispersion Spectra*

Dispersion spectra are recorded based on analyzing the differential detector signal  $\Delta I_{\text{rel}}$  while scanning the laser wavelength. As outlined above (compare Eq. 10 to Eq. 12),  $\Delta I_{\text{rel}}$  scales linearly with the sample's refractive index for sufficiently diluted samples. Therefore,  $\Delta I_{\text{rel}}$  immediately yields dispersion spectra if the interferometric phase is kept close to  $\frac{\pi}{2}$  (moving piezo method).

To record dispersion spectra independent from the small signal approximation (compare Eq. (11)), an alternative approach, coined “fixed piezo method”, was investigated.

*Moving Piezo Method.* Using this method, the relative phase between the two interferometric arms is actively compensated by the piezo-positioned mirror. To achieve this, the differential detector signal  $\Delta I_{\text{rel}}$  is digitized and supplied to a LabView internal PID-controller. The PID-controller keeps  $\Delta I_{\text{rel}} = 0$  by acting on the piezo element attached to mirror M1 via the piezo-controller. The working point of this measurement principle is indicated by the red circle in Figure 2. As the sample induced phase shift is continuously compensated by the piezo drive while scanning the laser wavelength, the corresponding piezo voltage is a direct measure of mirror displacement  $\delta$  and hence also of the sample’s refractive index. To record dispersion spectra of a sample, a background spectrum  $\delta_0(\tilde{\nu})$ , obtained for both flow cells filled with the solvent, must be subtracted from the sample spectrum. The non-zero background originates from the interferometric phase differing from  $\frac{\pi}{2}$  (see Eq. 10 and Figure 2) for all wavelengths except the center wavelength since  $\Delta l \neq \frac{\lambda}{4}$ , as well as from small deviations of the interferometer from perfect symmetry. All spectra, including dispersion spectra using the fixed piezo method (see below) and absorption spectra, were recorded at frequency steps of  $1 \text{ cm}^{-1}$  and an averaging time of 1 s per step. After subtraction of  $\delta_0(\tilde{\nu})$  from the sample spectrum  $\delta_{\text{spl}}(\tilde{\nu})$ , the refractive index difference  $\Delta n$  between sample and solvent is calculated from the background-free mirror displacement  $\delta(\tilde{\nu}) = \delta_{\text{spl}}(\tilde{\nu}) - \delta_0(\tilde{\nu})$  and the known film thickness  $d$  as (compare Eq. 4)

$$\Delta n(\tilde{\nu}) := n - n_0 = \frac{\delta(\tilde{\nu}) \cdot \sqrt{2}}{d} \quad (13)$$

The factor of  $\sqrt{2}$  appears due to geometric considerations, because the mirror travel is along the diagonal line between the mirrors M1 and M2. In case of known refractive index  $n_0$  of the reference solution in the wavenumber region of interest, an absolute refractive index spectrum can be determined. The main limitation of this approach in the current setup was the hysteresis effects of the piezo crystal, which limited the quality of the recorded piezo voltage as a measure of mirror displacement and limits the reproducibility of measurements. For this reason,

quantitative measurements were performed using the differential signal  $\Delta I_{\text{rel}}$  directly as a dispersion spectrum at a fixed mirror position.

*Fixed-Piezo Method.* When employing this method, the mirror displacement  $\delta$  is fixed to  $\frac{\lambda}{4}$  for the center wavelength throughout the measurement. To this end, the mirror displacement is adjusted until  $\Delta I_{\text{rel}} = 0$  while both flow cells are filled with the solvent. Next, a background spectrum  $\Delta I_{\text{rel},0}(\tilde{\nu})$  and sample spectrum are recorded as described above, but with fixed piezo position. From both spectra, a spectrum of displacement is calculated using Eq. 14:

$$\delta(\tilde{\nu}) = \frac{\lambda}{2\pi} \sin^{-1} \Delta I_{\text{rel}}(\tilde{\nu}) \quad (14)$$

which is derived from Eq. 11 by assuming  $A \approx 0$  (see Supplemental Material Figure S2). The resulting spectra of displacement are treated as described above to derive a spectrum of the refractive index  $\Delta n(\tilde{\nu})$  of the sample.

Besides overcoming the adverse hysteresis effects of the piezo crystal, this approach also allows increasing the scan speed. However, the spectrum of  $\Delta I_{\text{rel}}$  is recorded for an interferometric phase other than  $\frac{\pi}{2}$  for all wavelengths except the center wavelength since  $\delta \neq \frac{\lambda}{4}$ . This yields a non-zero background that depends also on the sample's absorption and makes measurements susceptible to laser intensity noise. Within the tuning range of the EC-QCL (1200  $\text{cm}^{-1}$  to 950  $\text{cm}^{-1}$ ), the phase varies by approximately  $\frac{\pi}{10}$  around 0. For high concentrations (large  $\Delta n$  and  $A$ ), this yields significant contributions from absorption to the recorded spectrum of  $\Delta I_{\text{rel}}$  and hence deviation from linearity of the obtained value with concentration.

*Absorption Spectroscopy.* For recording absorption spectra, the beam path in one of the two arms of the interferometer (here, the path passing FC1, Figure 1) is blocked so that no interference occurs. Reference and sample spectra  $I_0^A(\tilde{\nu})$  and  $I^A(\tilde{\nu})$  are measured by consecutively injecting the reference and the sample in FC2 and recording the sum of both detector signals. Absorption spectra are calculated as

$$A(\tilde{\nu}) = \log_{10} \left( \frac{I_0^A(\tilde{\nu})}{I^A(\tilde{\nu})} \right) \quad (15)$$

## Reagents and Samples

Sodium fluoride 99%, anhydrous and glucose, were purchased from Sigma Aldrich. Fructose 99%, sucrose 99%, and ethanol abs. were purchased from Merck. All samples were prepared in a 1% NaF solution to avoid corrosion of the BaF<sub>2</sub>-windows (Korth Kristalle GmbH, Germany) in contact with solvent caused by the small solubility of BaF<sub>2</sub> in water.

## RESULTS AND DISCUSSION

### *Qualitative Evaluation of the Recorded Spectra*

For qualitative evaluation of dispersion spectra recorded with the described setup, ethanol was chosen as an analyte. Ethanol features two separated and characteristic bands in the spectral emission region of the employed EC-QCL. The measured absorption and dispersion spectra of 5%v/v ethanol in water are shown in Figure 3b. For comparison, an FT-IR absorption spectrum was recorded, and a refractive index spectrum was calculated by the Kramers–Kronig transformation (Figure 3a). The absorption spectra show IR bands at 1046 and 1086 cm<sup>-1</sup> that are attributed to the asymmetric C–C–O stretching modes of the gauche and anti-conformers of ethanol.<sup>17,18</sup> The absorption spectrum recorded with the MZI setup agrees well with the FT-IR spectrum. Regarding the dispersion spectra recorded with the MZI, the general shape of the dispersion spectra agrees well with the Kramers–Kronig transformed FT-IR absorption spectra. Dispersion spectra show the characteristic shape of the refractive index close to an absorption band including a region of anomalous dispersion ( $\frac{dn}{d\lambda} > 0$ ) around the band center (see Figure 3b). Differences between the calculated spectrum and the dispersion spectrum recorded with fixed piezo position are expected since the strong absorption yields significant errors when using the approximation,  $A \approx 0$  (compare Eq. 12), as discussed above. The effect of this approximation on the retrieved dispersion spectrum is discussed in the supporting information (Figure S2). The slightly smaller excursion around resonance in the dispersion spectrum measured with moving piezo method as compared to the calculated spectrum might point to an insufficient speed of the feedback loop and will be investigated in the future. For both methods, two kinds of deviation of

optical components from assumptions taken above can affect the measurements. Firstly, the reflectivity and transmission of the beam splitters is not  $R = T = 0.5$  as assumed in Eq. 10 for the whole spectral range (see datasheet of the used ThorLabs ZnSe beam splitter BSW710).

Secondly, the response of the two detectors must be equal to justify the insertion of the detector signal for  $I_{out,1}$  and  $I_{out,2}$  in the equations above without scaling. Differences in detector response may arise during amplification of detector signals and from the optical alignment of the beams on the detectors. Differences might also be associated with insufficient temperature stabilization of the current setup. Assuming a temperature change of 1 K and a diameter of the interferometer of 0.25 m, the linear heat expansion coefficient of the aluminum breadboard results in a change of the overall diameter of around  $5 \mu\text{m}$ ,<sup>19</sup> which is much larger than the sample induced displacements  $\delta(\tilde{\nu})$ .

#### *Quantitative Analysis of the Acquired Spectra*

Experimentally, an offset between consecutively recorded dispersion spectra was observed, most likely due to temperature instabilities and heat expansion of the used optical components. Thus, for obtaining calibration curves, the slopes of the dispersion spectrum in the points of inflection were used, as illustrated in Figure S1. These points coincide with the band maxima in the corresponding absorption spectra. For evaluation of the slopes, a custom-made Matlab routine was programmed. The routine uses the known wavenumber values of the absorption band and calculates an average slope using the four data points next to these wavenumber values. The slope values found in this way were finally averaged to obtain the slope values used for calibration.

#### *Univariate Quantification Employing Absorption and Dispersion Spectra*

In order to evaluate the capabilities of the MZI setup for quantification purposes, absorption and dispersion measurements were performed. To this end, glucose solutions were prepared with concentrations ranging between 2 and  $10 \text{ g L}^{-1}$ . The recorded absorption spectra used as a reference for the dispersion spectroscopy measurements are shown in Figure 4a. Characteristic IR bands at 994, 1036, 1081, 1108, and  $1153 \text{ cm}^{-1}$  can be assigned to C–O stretching, C–C stretching as well as C–O–H bending modes of the glucose molecule.<sup>20</sup> For quantitative analysis, the band height was evaluated at the most prominent IR absorption band at  $1036 \text{ cm}^{-1}$ . The

calibration curve (inset in Figure 4a) indicates that the experimental data fit well to a linear regression line. By evaluation of the slope  $dA(1036\text{ cm}^{-1})/dc$  and the root mean square noise level  $\sigma_{RMS}$  the relevant spectral region, the limit of detection was calculated as  $c_{LOD,A} = 3 \frac{\sigma_{RMS}}{dA/dc} = 0.19\text{ g L}^{-1}$ . Quantitative measurements using dispersion spectroscopy were exclusively performed employing the fixed-piezo method, due to aberrations introduced by hysteresis effects of the piezo element when using the moving piezo method, as outlined in the experimental section. For quantitative evaluation of the dispersion spectra, the slopes of the tangents at the inflection points were evaluated (Figure S1). The obtained calibration curve (Figure 4b, inset) confirms the expected linearity with concentration. For dispersion spectra, the limit of detection was evaluated to be  $0.53\text{ g L}^{-1}$ . These measurements and quantitative analysis demonstrate that both absorption and dispersion spectra can be employed for quantitative measurements and that the recorded dispersion spectra show the expected linear behavior with concentration.

#### *Multivariate Quantification of Glucose, Fructose and Sucrose Employing Absorption and Dispersion Spectra*

In order to test the capabilities of the developed setup for quantification of complex analyte mixtures, tertiary solutions containing glucose, fructose and sucrose were analyzed. Simultaneous quantification of these sugars in different matrices (e.g., fruit juices, honey) is routinely performed using FT-IR spectroscopy,<sup>21–24</sup> thus it poses an excellent problem to benchmark the performance of the developed method. A calibration data set comprising 17 solutions was prepared with individual sugar concentrations ranging between 1 and  $10\text{ g L}^{-1}$  (Table S1) and absorption as well as dispersion spectra were recorded. Within the observed spectral region, the absorption bands of glucose, fructose and sucrose strongly overlap. To tackle quantification in this multicomponent system, multivariate partial least squares (PLS) regression models were optimized for each analyte (PLS Toolbox 8.0, Eigenvector Research Inc.). The PLS calibration parameters and internal figures of merit are summarized in Table I. For all PLS models, three latent variables were used, reflecting the three components in the solution. Coefficients of determination ( $R^2$ ) of calibration and leave-one-out cross-validation are  $>0.999$  and  $>0.998$  for absorption and dispersion spectra, respectively, for all three sugars. The root mean square error of calibration (RMSEC) and cross-validation (RMSECV) range between 0.04

and  $0.05 \text{ g L}^{-1}$  and  $0.05$  and  $0.07 \text{ g L}^{-1}$ , for absorption and between  $0.06$  and  $0.11 \text{ g L}^{-1}$  and  $0.08$  and  $0.22 \text{ g L}^{-1}$  for dispersion spectra, respectively, while the bias of cross validation (CV bias) as a measure of accuracy range between  $-0.037$  and  $0.01 \text{ g L}^{-1}$  respectively. Overall, both absorption and dispersion spectroscopy allow simultaneous quantification of the three sugars at few percent accuracy as determined from the cross validation. The slightly, but actual better figures of merit found for absorption spectra most likely originate from the higher experimental sensitivity of dispersion spectroscopy with the current implementation to external, environmental fluctuations, as described in the previous sections.

## CONCLUSION

In this work, a Mach–Zehnder interferometry setup was introduced for recording mid-IR dispersion spectra of liquid samples using an EC-QCL. After a thorough discussion of the theoretical basis and principles of signal generation, two methods were introduced for the acquisition of dispersion spectra. Qualitative comparison of the shape of the measured dispersion spectra delivered comparable results with state-of-the-art FT-IR measurements concerning absorption and Kramers–Kronig transformed refractive index spectra. Quantitative analysis was performed employing dispersion spectra for a calibration of glucose in water and results were compared with conventional absorption spectroscopy. The calibration results confirm the expected linearity of dispersion spectra with concentration and compare well with calibration based on absorption spectroscopy. We introduced two methods of recording dispersion spectra. The spectra obtained with the moving piezo method agree very well with theory, while spectra recorded with fixed piezo method have the advantage of higher reproducibility. PLS based multivariate calibration of solutions containing three different sugars were performed based on dispersion spectra and referenced against results obtained from absorption spectroscopy. The RMSECV of only a few percent of the actual concentrations as well as other figures of merit are very similar to absorption spectroscopic results and demonstrate the potential of mid-IR dispersion spectroscopy for solving complex analytical problems at high accuracy based on the rich spectroscopic information of this spectral region.

In conclusion, this work demonstrates that mid-IR dispersion spectroscopy is an interesting alternative to state-of-the-art absorption spectroscopy not only for gases,<sup>1,13</sup> but also

for liquid samples. Experimental drawbacks identified during this proof-of-concept work were the high susceptibility of the interferometric approach to temperature fluctuations of the optical components. Planned measures to overcome these issues include the implementation of an improved temperature stabilization of the interferometer to avoid temperature drifts and decrease phase noise of the interferometer. This is crucial to obtain consistent dispersion spectra. Also, further miniaturizations of the setup are planned. While the linearity of recorded signals with concentration in dispersion spectroscopy could already be successfully demonstrated, further improvements of the experimental setup promise to also harness dispersion spectroscopy's robustness against laser intensity noise and to increase sensitivity.

### **ACKNOWLEDGMENTS**

This work has received funding from the European Union's Horizon 2020 research and innovation programme under grant agreement No 780240 and from the COMET Centre CHASE (project No 868615), which is funded within the framework of COMET (Competence Centers for Excellent Technologies) by BMVIT, BMDW, the Federal Provinces of Upper Austria and Vienna. The COMET programme is run by the Austrian Research Promotion Agency (FFG). M.G.C. acknowledges the Ministry of Education, Culture and Sports (FPU15/03119 fellowship) for a mobility grant during her doctorate studies.

### **SUPPLEMENTAL MATERIAL**

All supplemental material mentioned in the text is available in the online version of the journal.

### **CONFLICT OF INTEREST**

The authors declare no competing interest.

### **REFERENCES**

1. M. Nikodem, G. Wysocki. "Molecular Dispersion Spectroscopy—New Capabilities in Laser Chemical Sensing". *Ann. N.Y. Acad. Sci.* 2012. 1260(1): 101–111.
2. P. Hoffmann, E. Knoezinger. "Dynamic Range Problems in Fourier Transform IR and Far-IR Spectroscopy". *Appl. Spectrosc.* 1987. 41(8): 1303–1306.
3. D.B. Chase. "Nonlinear Detector Response in FT-IR". *Appl. Spectrosc.* 1984. 38(4): 491–494.

4. M.J. Weida, B. Yee. "Quantum Cascade Laser-Based Replacement for FT-IR Microscopy". *Proc. SPIE 7902, Imaging, Manipulation, and Analysis of Biomolecules, Cells, and Tissues IX*, 79021C. 2011. <https://doi.org/10.1117/12.873954>.
5. A. Schwaighofer, M. Brandstetter, B. Lendl. "Quantum Cascade Lasers (QCLs) in Biomedical Spectroscopy". *Chem. Soc. Rev.* 2017. 46(19): 5903–5924.
6. B. Lendl, J. Frank, R. Schindler, A. Müller, et al. "Mid-Infrared Quantum Cascade Lasers for Flow Injection Analysis". *Anal. Chem.* 2000. 72(7): 1645–1648.
7. M. Brandstetter, A. Genner, K. Anic, B. Lendl. "Tunable External Cavity Quantum Cascade Laser for the simultaneous Determination of Glucose and Lactate in Aqueous Phase". *Analyst.* 2010. 135(12): 3260–3265.
8. M.R. Alcaráz, A. Schwaighofer, C. Kristament, G. Ramer, et al. "External-Cavity Quantum Cascade Laser Spectroscopy for Mid-IR Transmission Measurements of Proteins in Aqueous Solution". *Anal. Chem.* 2015. 87(13): 6980–6987.
9. A. Schwaighofer, M.R. Alcaráz, C. Araman, H. Goicoechea, B. Lendl. "External Cavity-Quantum Cascade Laser Infrared Spectroscopy for Secondary Structure Analysis of Proteins at Low Concentrations". *Sci. Rep.* 2016. 6: 33556.
10. A. Schwaighofer, M. Montemurro, S. Freitag, C. Kristament, et al. "Beyond Fourier Transform Infrared Spectroscopy: External Cavity Quantum Cascade Laser-Based Mid-Infrared Transmission Spectroscopy of Proteins in the Amide I and Amide II Region". *Anal. Chem.* 2018. 90(11): 7072–7079.
11. J. Hayden, S. Hugger, F. Fuchs, B. Lendl. "A Quantum Cascade Laser-Based Mach–Zehnder Interferometer for Chemical Sensing Employing Molecular Absorption and Dispersion". *Appl. Phys. B: Lasers Opt.* 2018. 124(2): 1–9.
12. G. Wysocki, D. Weidmann. "Molecular Dispersion Spectroscopy for Chemical Sensing Using Chirped Mid-Infrared Quantum Cascade Laser". *Opt. Express.* 2010. 18(25): 26123.
13. P. Martín-Mateos, J. Hayden, P. Acedo, B. Lendl. "Heterodyne Phase-Sensitive Dispersion Spectroscopy in the Mid-Infrared with a Quantum Cascade Laser". *Anal. Chem.* 2017. 89(11): 5916–5922.
14. P. Kozma, F. Kehl, E. Ehrentreich-Förster, C. Stamm, F.F. Bier. "Integrated Planar Optical Waveguide Interferometer Biosensors: A Comparative Review". *Biosens. Bioelectron.*

2014. 58: 287–307.
15. Q. Liu, X. Tu, K.W. Kim, J.S. Kee, et al. “Highly Sensitive Mach-Zehnder Interferometer Biosensor Based on Silicon Nitride Slot Waveguide”. *Sens. Actuators, B*. 2013. 188: 681–688.
  16. M. Sieger, F. Balluff, X. Wang, S.S. Kim, et al. “On-Chip Integrated Mid-Infrared GaAs/AlGaAs Mach-Zehnder Interferometer”. *Anal. Chem.* 2013. 85(6): 3050–3052.
  17. S. Corsetti, F.M. Zehentbauer, D. McGloin, J. Kiefer. “Characterization of Gasoline/Ethanol Blends by Infrared and Excess Infrared Spectroscopy”. *Fuel*. 2015. 141: 136–142.
  18. M.K. Ahmed, S. Ali, E. Wojcik. “The C–O Stretching Infrared Band as a Probe of Hydrogen Bonding in Ethanol-Water and Methanol-Water Mixtures”. *Spectrosc. Lett.* 2012. 45(6): 420–423.
  19. A.J.C. Wilson. “The Thermal Expansion of Aluminium from 0° to 650 °C”. *Proc. Phys. Soc.* 1941. 53(3): 235–244.
  20. M. Kačuráková, M. Mathlouthi. “FT-IR and Laser-Raman Spectra of Oligosaccharides in Water: Characterization of the Glycosidic Bond”. *Carbohydr. Res.* 1996. 284(2): 145–157.
  21. L.F. Leopold, N. Leopold, H.A. Diehl, C. Socaciu. “Quantification of Carbohydrates in Fruit Juices Using FT-IR Spectroscopy and Multivariate Analysis”. *Spectroscopy*. 2011. 26(2): 93–104.
  22. F. Cadet, C. Robert, B. Offmann. “Simultaneous Determination of Sugars by Multivariate Analysis Applied to Mid-Infrared Spectra of Biological Samples”. *Appl. Spectrosc.* 1997. 51(3): 369–375.
  23. I.F. Duarte, A. Barros, I. Delgadillo, C. Almeida, A.M. Gil. “Application of FT-IR Spectroscopy for the Quantification of Sugars in Mango Juice as a Function of Ripening”. *J. Agric. Food Chem.* 2002. 50(11): 3104–3111.
  24. J. Wang, M.M. Kliks, S. Jun, M. Jackson, Q.X. Li. “Rapid Analysis of Glucose, Fructose, Sucrose, and Maltose in Honeys from Different Geographic Regions Using Fourier Transform Infrared Spectroscopy and Multivariate Analysis”. *J. Food Sci.* 2010. 75(2): C208–C214.



M1, M2 protected gold mirrors, which form the Mach–Zehnder interferometer. M2 is attached to a piezo drive to adjust the path lengths of the two part-beams. FC1 and FC2 are the BaF<sub>2</sub> liquid flow cells with 50 μm thickness. The parabolic focusing mirrors PM1 and PM2 are employed to focus the beams on the pyroelectric detectors D1 and D2, respectively.

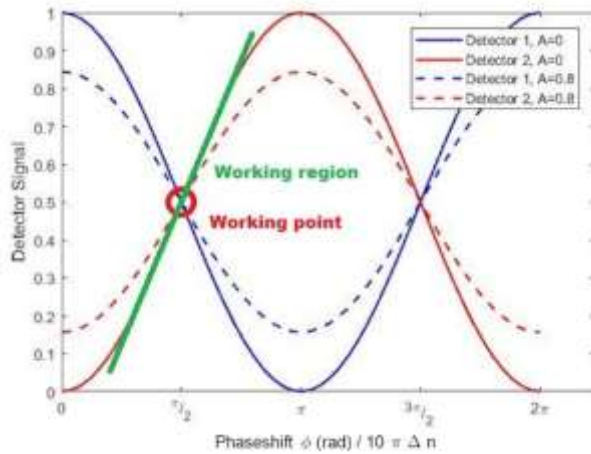


**Figure 2.** Visualization of the measurement principles for recording dispersion spectra. The figure shows the behaviour of the normalized detector signals corresponding to  $I_{out,1}$  and  $I_{out,2}$  (compare Eqs. 8 and 9), normalized by the sum of  $I_{out,1}$  and  $I_{out,2}$  with phase shift  $\phi = \frac{2\pi}{\lambda}(n - n_0)d$ . With the used cell thickness of 50 μm and an average wavelength of 10 μm, this phase shift represents the difference in refractive index  $\Delta n = n - n_0$  times  $10\pi$ . The detector signals are plotted for  $A = 0$  and  $A = 0.8$ , respectively. The red circle and the green line illustrate the working regions of the two different measurement methods (moving and fixed piezo method) described in the next sections.

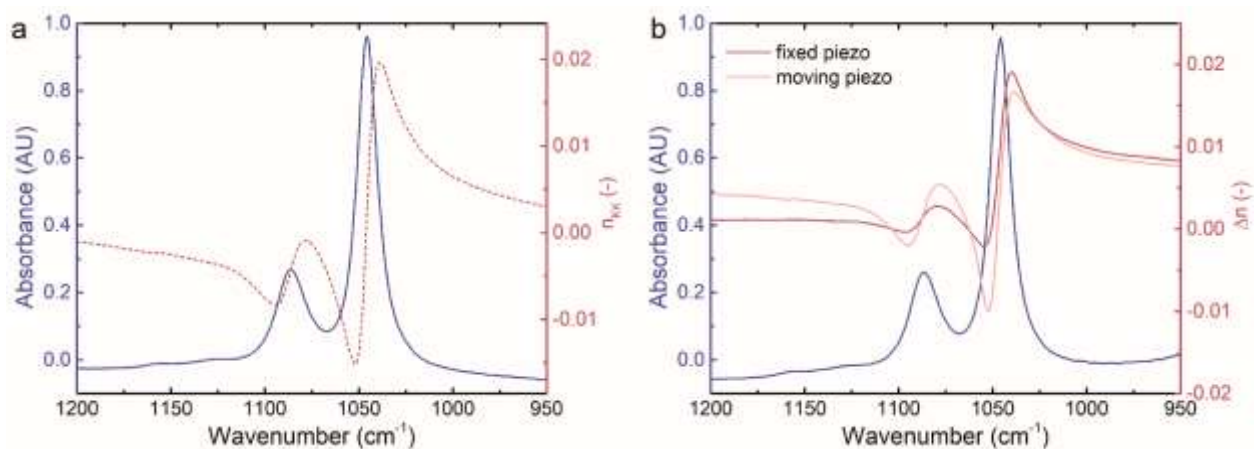


**Figure 3.** (a) Absorption spectrum (blue) of 5% ethanol recorded using FT-IR spectroscopy. The refractive index spectrum (red dashed) was calculated by Kramers–Kronig transformation (performed with in-house code developed in Matlab v.R2014b). (b) Absorption (blue) and refractive index spectra of 5% ethanol recorded by the moving-piezo (light red) and fixed-piezo (red) method with the developed Mach–Zehnder interferometer setup.

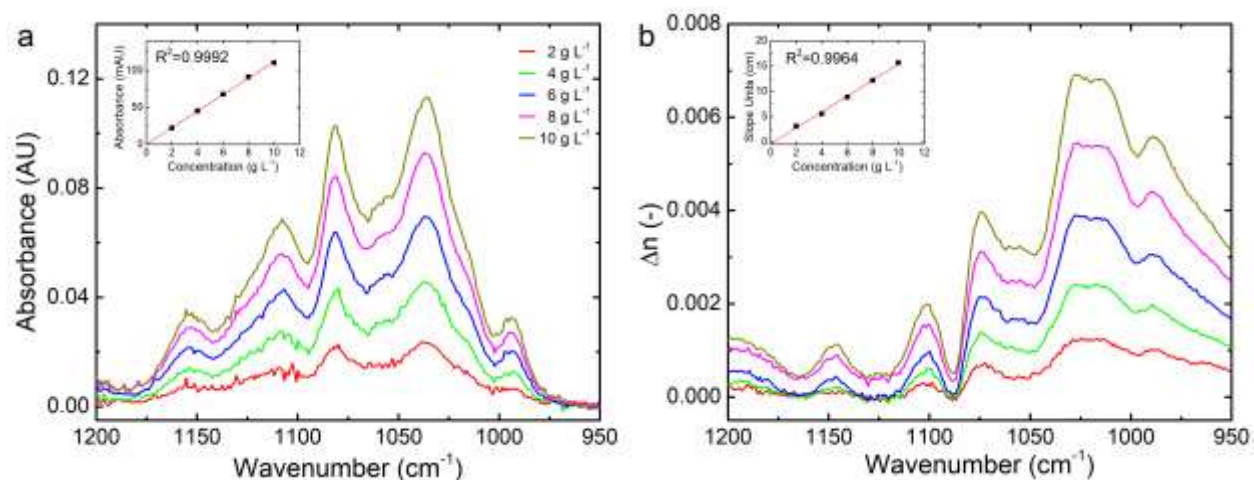


**Figure 4.** (a) Absorption spectra of glucose recorded with the MZI. Inset shows univariate calibration evaluated at 1036 cm<sup>-1</sup>. Refractive index spectra of glucose recorded with (b) fixed-piezo method using the MZI. Insets show univariate calibration by evaluation of the slopes at the points of inflection.

## Supplemental Material

### External Cavity Quantum Cascade Laser-Based Mid-Infrared Dispersion Spectroscopy for Qualitative and Quantitative Analysis of Liquid-Phase Samples

Stefan Lindner<sup>1</sup>, Jakob Hayden<sup>1</sup>, Andreas Schwaighofer<sup>1</sup>, Tobias Wolflehner<sup>1</sup>,  
Christian Kristament<sup>1</sup>, María González-Cabrera<sup>2</sup>, Stefan Zlabinger<sup>1</sup>, and Bernhard Lendl<sup>1\*</sup>

<sup>1</sup> Institute of Chemical Technologies and Analytics, Vienna University of Technology, Getreide-  
markt 9/164-UPA, 1060 Vienna, Austria

<sup>2</sup> Department of Physical and Analytical Chemistry, Universidad de Jaén, Campus Las  
Lagunillas, s/n, 23071, Jaén, Spain

**Corresponding author email:** [Bernhard.lendl@tuwien.ac.at](mailto:Bernhard.lendl@tuwien.ac.at)

#### Table of Contents

Quantification method using dispersion spectra .....	S20
Sugar concentration table for quantitative analysis .....	S21
FT-IR reference measurements .....	S22
Influence of the mathematical approximations for obtaining dispersion spectra .....	S22

## Quantification Method Using Dispersion Spectra

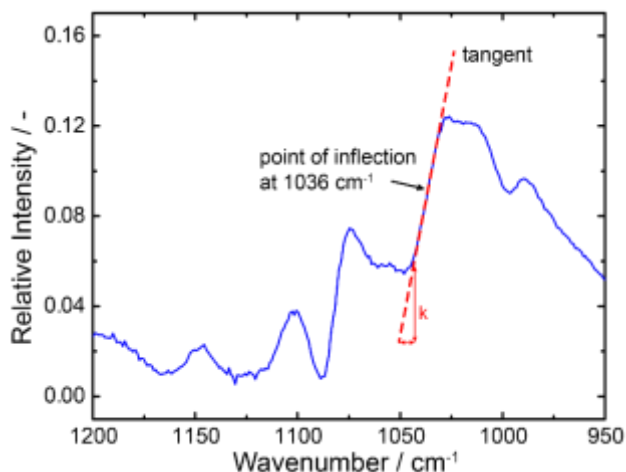


**Figure S1.** Illustration of the approach used for evaluation of the slopes of inflection points for quantification with dispersion spectra. To find stable slope values, not only the slope in the point of inflection itself, but also the slopes in the four points surrounding it are calculated and averaged. The average slope of all significant points of inflection (corresponding to the main absorption bands) is taken as signal for analyte quantification.

**Sugar Concentration Table for Quantitative Analysis****Table S1.** Sugar concentrations employed for preparing the calibration set for PLS analysis.

	Fructose	Glucose	Sucrose
C1	5.5	10	5.5
C2	8.2	2.8	2.8
C3	5.5	5.5	5.5
C4	10	5.5	5.5
C5	5.5	5.5	5.5
C6	5.5	5.5	10
C7	5.5	5.5	5.5
C8	2.8	8.2	2.8
C9	8.2	2.8	8.2
C10	5.5	1	5.5
C11	2.8	2.8	2.8
C12	5.5	5.5	1
C13	2.8	2.8	8.2
C14	8.2	8.2	2.8
C15	8.2	8.2	8.2
C16	2.8	8.2	8.2
C17	1	5.5	5.5

### FT-IR Reference Measurements

FT-IR absorption measurements were performed using a Bruker Tensor 37 FT-IR spectrometer (Ettlingen, Germany) equipped with a liquid nitrogen cooled HgCdTe (mercury cadmium telluride) detector. The samples were placed between two BaF<sub>2</sub> windows separated by a 50 µm-thick spacer. Spectra were acquired with a spectral resolution of 4 cm<sup>-1</sup> in double-sided acquisition mode. A total of 16 scans were averaged per spectrum, which was calculated using a Blackman-Harris 3-term apodization function and a zero filling factor of 2. All spectra were acquired at 25 °C. Spectra were analyzed using the software package OPUS 7.2 (Bruker, Ettlingen, Germany).

### Influence of the Mathematical Approximations for Obtaining Dispersion Spectra

Several mathematical approximations of the equations describing the emerging of dispersion spectra were done. The assumption  $A = 0$ , was done, so we assumed that there is no absorption when acquiring dispersion spectra. At and around the absorption peaks of ethanol shown in Figure 3, this approximation does not hold. The effect of this deviation is shown in Figure S2. Here, spectra of  $\Delta n = n - n_0$  were calculated from the measured spectra of  $\Delta I_{\text{rel},0}(\tilde{\nu})$ ,  $\Delta I_{\text{rel}}(\tilde{\nu})$  and  $A(\tilde{\nu})$  of 5% aqueous solution of ethanol using the non-approximate Eq. 10. With the background spectrum  $\Delta I_{\text{rel},0}(\tilde{\nu})$  and the fact that in theory there is no difference in the refractive index when the flowcells both are filled with solvent, a spectrum of geometric phase shift  $\Delta l(\tilde{\nu})$  is recorded.

$$\Delta l(\tilde{\nu}) = \frac{\lambda}{2\pi} \cos^{-1} \left( \frac{1}{2} \left( 10^{\frac{\tilde{A}}{2}} + 10^{-\frac{\tilde{A}}{2}} \right) \Delta I_{\text{rel},0}(\tilde{\nu}) \right)$$

This in combination with the recorded spectrum  $\Delta I_{\text{rel}}(\tilde{\nu})$  of the sample is used to calculate the refractive index spectrum  $\Delta n(\tilde{\nu})$ .

$$\Delta n(\tilde{\nu}) = \frac{1}{d} \left[ \frac{\lambda}{2\pi} \cos^{-1} \left( \frac{1}{2} \left( 10^{\frac{\tilde{A}}{2}} + 10^{-\frac{\tilde{A}}{2}} \right) \Delta I_{\text{rel}}(\tilde{\nu}) \right) - \Delta l(\tilde{\nu}) \right]$$

Inserting the scaled absorption spectrum  $\tilde{A} = \alpha A$  with scaling factor  $\alpha \in [0,1] \cap \mathbb{R}$ , allows studying the effect of absorption on the retrieved refractive index spectrum, with  $\alpha = 0$  corresponding to the approximate solution shown in Figure 3 and with  $\alpha = 1$  to the exact solution.

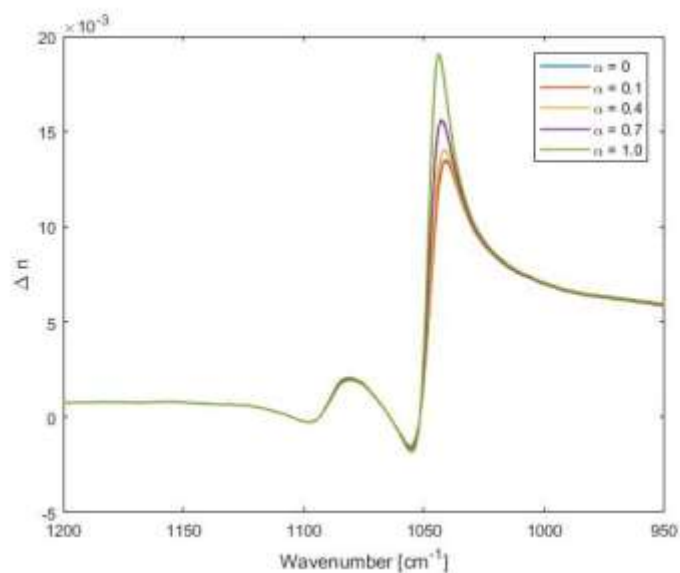


**Figure S2.** Illustration of the influence of the dispersion spectrum measured using the fixed piezo method. The attenuation factor  $\alpha$  has been set to values from 1 to 0.05 to show the convergence to the used approximation  $A = 0$  in our work. For  $\alpha = 0.1$  there is already a full overlap with the blue line of the  $A = 0$  approximation, so that this line does not show up.